

Standard and helical magnetorotational instability

How singularities create paradoxal phenomena in MHD

Oleg N. Kirillov · Frank Stefani

Received: date / Accepted: date

Abstract The magnetorotational instability (MRI) triggers turbulence and enables outward transport of angular momentum in hydrodynamically stable rotating shear flows, e.g., in accretion disks. What laws of differential rotation are susceptible to the destabilization by axial, azimuthal, or helical magnetic field? The answer to this question, which is vital for astrophysical and experimental applications, inevitably leads to the study of spectral and geometrical singularities on the instability threshold. The singularities provide a connection between seemingly discontinuous stability criteria and thus explain several paradoxes in the theory of MRI that were poorly understood since the 1950s.

Keywords Rotating shear flow · Couette-Taylor flow · accretion disk · magnetorotational instability · WKB · Plücker conoid · exceptional point

1 Introduction

In 1890 Maurice Couette, a student of Gabriel Lippmann and Joseph Boussinesq, defended his thesis “Études sur le frottement des liquides” and was awarded his doctorate at the Sorbonne “with all white balls” and *cum laude* for the experiments with a viscometer of his own design [1, 2, 3]. Seventy years later Evgeny Velikhov, then a physics student of Stanislav Braginsky at the

O.N. Kirillov
Helmholtz-Zentrum Dresden-Rossendorf
P.O. Box 510119, D-01314 Dresden, Germany
Tel.: +49-351-2602154
E-mail: o.kirillov@hzdr.de

F. Stefani
Helmholtz-Zentrum Dresden-Rossendorf
P.O. Box 510119, D-01314 Dresden, Germany
Tel.: +49-351-2603069
E-mail: f.stefani@hzdr.de

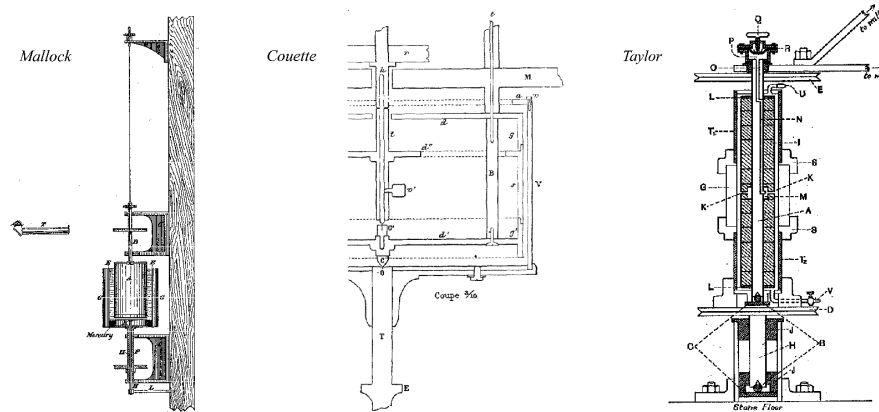


Fig. 1 Original drawings of the viscometers of (left) Mallock [7,8] with either outer or inner rotating cylinder and (center) Couette [1,3] with rotating outer cylinder and (right) the experimental apparatus of Taylor [5] in which both cylinders could rotate.

M.V. Lomonosov Moscow State University, discovered the magnetorotational instability of the Couette-Taylor flow [4].

The fates of the first scientific works of both young scientists were similar in a sense that the reaction of the scientific community in both cases was quiescent for almost 30 years, until Geoffrey Taylor investigated stability of the rotating Couette flow in 1923 [5] and Steven Balbus and John Hawley demonstrated in 1991 the crucial role of the magnetorotational instability for the explanation of transition to turbulence and thus the anomalous viscosity in accretion disks surrounding gravitating bodies [6].

The aim of Couette was to measure the kinematic viscosity of water. In 1888 [2] he reported on the design of a viscometer that he presented at the 1889 Universal Exhibition in Paris [1]. In the Couette viscometer the liquid occupied a space between two co-axial cylinders, the outer one rotating while the inner one fixed, Fig. 1. Couette found that at small speeds of rotation the moment of the drag which the fluid exerted on the inner cylinder was indeed proportional to the velocity of the outer cylinder, from which the kinematic viscosity was determined. At higher speeds the drag increased at a greater rate than the velocity, indicating the onset of turbulent motion.

In his thesis Couette referred [1] to the work of Arnulph Mallock from Rayleigh's laboratory [7] who independently designed a similar device with either the inner or the outer cylinder rotating, Fig. 1. Mallock confirmed Couette's results, but in the case when the inner cylinder rotated and the outer one not, he surprisingly observed instability of the fluid at all speeds that he used [7,8]. Although the effect had been anticipated by Stokes already in 1848 [9], it was explained (in the inviscid approximation) by Rayleigh only in 1917 [10]. According to Rayleigh's criterion, an inviscid rotating flow is stable with respect to axisymmetric perturbations provided that its angular momentum

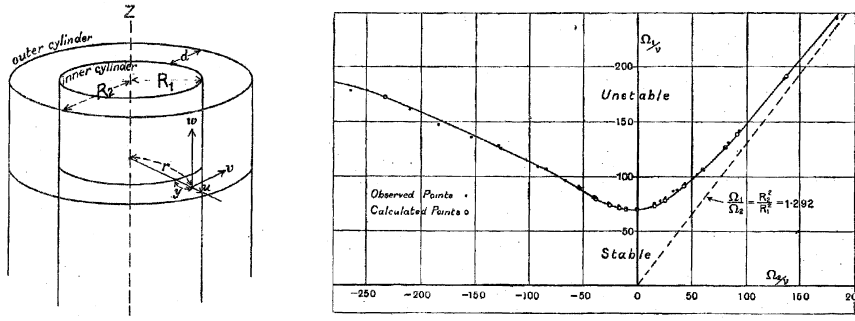


Fig. 2 Original drawings of the geometry of the Taylor's model and of the stability diagram in the $(\Omega_2/\nu, \Omega_1/\nu)$ -plane for $R_1 = 3.55$ cm and $R_2 = 4.035$ cm [5]. Dashed line is the Rayleigh's inviscid stability boundary [10].

increases radially

$$\frac{1}{R^3} \frac{d}{dR} (\Omega R^2)^2 > 0. \quad (1)$$

When this criterion is not fulfilled, the balance between the centrifugal force and a pressure gradient is broken and the flow is centrifugally unstable. In particular, the inviscid fluid between two co-rotating and co-axial cylinders of infinite lengths and radii $R_1 < R_2$ is unstable if and only if

$$\Omega_1 R_1^2 > \Omega_2 R_2^2, \quad (2)$$

where Ω_1 and Ω_2 are the angular velocities of the inner and outer cylinders, respectively, see Fig. 2.

Limitations in the design of the experiments by Couette and Mallock did not allow the full verification of the criterion (2). Besides, the steady flow in their viscometers was not close enough to two-dimensional because of relatively small length-to-diameter ratio. This motivated Geoffrey Taylor to construct a slimmer Couette cell making both co-rotation and counter-rotation of the cylinders possible, Fig. 1. In his 1923 work [5] Taylor performed a linear stability analysis of the Navier-Stokes equations in case of infinite length cylinders and managed to find a stability diagram in the $(\Omega_2/\nu, \Omega_1/\nu)$ -plane, see Fig. 2. It turned out that the viscosity, ν , modifies the Rayleigh criterion in such a manner that it becomes only a sufficient stability condition and that the viscous stability boundary asymptotically tends to the Rayleigh line in case of the co-rotating cylinders, Fig. 2. Moreover, the viscous flow is stable at small speeds of the inner cylinder when the outer one is at rest or in motion, while it inevitably becomes unstable when the velocity of the inner cylinder exceeds a critical value. This is in contradiction with the observations of Couette and Mallock that the viscous flow becomes unstable for large velocities of the outer cylinder when the inner does not move and is unstable at all speeds of the inner cylinder when the outer is at rest. The latter discrepancy is due to the fact that Mallock's lowest speed of rotation, 2 rpm, was still larger than the critical value calculated for the size of the cylinders he used [9] while the former

is essentially caused by the insufficient axial elongation of the viscometers of Mallock and Couette.

The stability boundary extracted from Taylor's experimental data [5] perfectly agreed with that followed from his linear stability analysis, Fig. 2. Furthermore, Taylor's experiments revealed that with the violation of the stability threshold, the rotating Couette flow bifurcates to a secondary steady state characterized by counter-rotating toroidal vortices (the Taylor vortex flow). Extending the parameters deeper inside the instability domain results in flows with even more complicated spatiotemporal patterns [5, 11]. Therefore, the instability of the Couette-Taylor (CT) flow is analogous to the static (divergence) instability in structural mechanics [12].

The excellent correspondence that Taylor obtained between theory and experiment demonstrated the correctness of the Navier-Stokes equations and of the no-slip boundary condition for the fluid at the cylinder walls [9] as well as it proved the applicability of linear stability analysis to the CT-flow. After the influential work [5], Couette-Taylor cells became a standard equipment for laboratory testing hydrodynamical and magnetohydrodynamical theories.

In 1953 Chandrasekhar first considered the CT-flow of a weakly electrically conducting viscous fluid in the presence of the uniform magnetic field that is parallel to the axis of rotation of the cylinders [13]. He demonstrated that in this case characterized by the very small ratio of the kinematic viscosity coefficient, ν , to the magnetic diffusivity coefficient, η , i.e. by the magnetic Prandtl number $Pm := \nu\eta^{-1} \ll 1$, the magnetic field stabilizes the hydrodynamically unstable CT-flow [13]. The article of Chandrasekhar has been brought to the attention of Evgeny Velikhov by his supervisor Stanislav Braginsky who posed a problem on the influence of the axial magnetic field on the hydrodynamically stable CT-flow—the very question that had not been addressed in [13].

In contrast to Chandrasekhar, Velikhov assumed that the liquid is both inviscid and perfectly conducting. In 1959 he established a new sufficient criterion of stability with respect to the axisymmetric perturbations in the form

$$\frac{d\Omega^2}{dR} > 0, \quad (3)$$

or, in terms of the angular velocities of the cylinders,

$$\Omega_2 > \Omega_1, \quad (4)$$

see the left panel of Fig. 3. In a subsequent work of 1960 Chandrasekhar confirmed this result [16].

Both Velikhov and Chandrasekhar pointed out that the new stability conditions (3) and (4) do not depend on the magnetic field strength B which implies that in the limit $B \rightarrow 0$ they do not converge to the Rayleigh's criteria (1) and (2) valid for $B = 0$, as is illustrated by the left panel of Fig. 3. In presence of dissipation the convergence is possible [17, 18, 19, 20, 21]. This dependence of the instability threshold on the sequence of taking the two limits of vanishing magnetic field and vanishing electrical resistivity constitutes

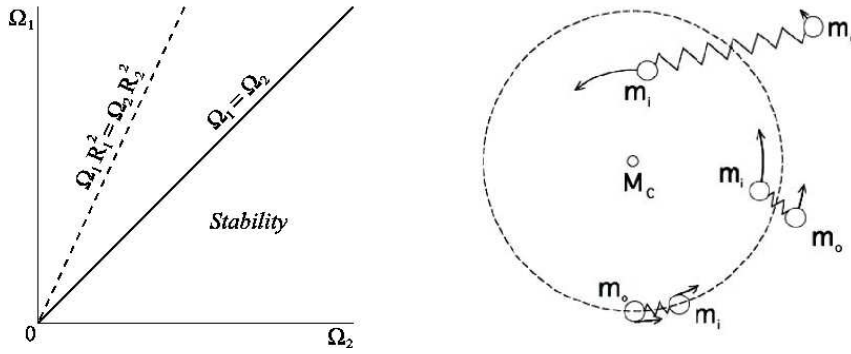


Fig. 3 (left) A diagram of stability with respect to axisymmetric perturbations of the Couette-Taylor flow of ideally electrically conducting inviscid fluid with an axial magnetic field applied [4]; dashed line is Rayleigh’s inviscid stability boundary [10]. (right) A paradigmatic mechanism of magnetorotational instability in accretion disks [15]. The action of the magnetic field is equivalent to that of elastic springs that lead to the exchange of angular momentum between the fast inner mass m_i and the slow outer mass m_o .

the famous *Velikhov-Chandrasekhar paradox*. Its physical explanation has been given in terms of Alfvén’s theorem [14] that in a fluid of zero resistivity the magnetic field lines are frozen-in to the fluid, independent on the strength of the magnetic field [4, 16].

Even half a century after the publications of Velikhov and Chandrasekhar the ‘dubious’ jump in the threshold of the *magnetorotational instability* (MRI) has not been fully understood and the paradox remained unresolved [21, 22, 23, 24, 25, 26] despite “much of the fluid and stellar community was aware of the instability, however, and of its curious behavior of ostensibly changing the Rayleigh criterion discontinuously” [22]. Maybe this is not so surprising when taking into account that even the astrophysical relevance of MRI to destabilize a differentially rotating flow in accretion disks around gravitating celestial bodies remained underappreciated during a long period until it was rehabilitated by Balbus and Hawley in 1991.

The central problem here is that accretion disks typically rotate according to Kepler’s law, $\Omega(R) \sim R^{-3/2}$ which results in an angular momentum $R^2\Omega(R) \sim R^{1/2}$ that fulfills Rayleigh’s stability criterion (1). Such stable, non-turbulent disks would not allow the outward directed angular momentum transport that is necessary for the infalling disk matter to accrete into the central object. In their seminal paper [6], Balbus and Hawley had highlighted the key role of the MRI in this process by showing that a weak, externally applied magnetic field is a trigger for the instability that actually taps into the rotational energy of the flow.

In the perfectly conducting fluid, the magnetic field lines are ‘frozen’ into it tethering fluid elements like a spring [22, 27], see Fig. 3(right). If such a couple is perturbed, the magnetic ‘tether’ retards the faster inner element that has to move to the lower Keplerian orbit and simultaneously it accelerates the slower outer fluid element that thus has to move to the higher orbit. The separation

between the elements grows with time yielding instability. Remarkably, this simple mechanical analogue of MRI proposed by Balbus and Hawley [6, 22, 27], is a working principle of numerous engineering projects developed since 1960s that involve momentum exchange tethers for the orbital transfer of satellites [28]. Well-known is instability of the orbiting ring of connected satellites as well as of the orbiting flexible and extensible ring in the context of studies of formation of planetary rings [29, 30].

In the reference frame comoving with a small patch of the magnetized accretion disk and rotating at the angular velocity $\Omega_0 = \Omega(R_0)$, the leading order WKB equations governing the evolution of its local radial (x) and azimuthal (y) displacements in the vicinity of a fiducial point with the radius R_0 , are [22]

$$\begin{aligned} \ddot{x} - 2\Omega_0\dot{y} + \left(R_0 \frac{d\Omega^2}{dR} \Big|_{R=R_0} + \omega_A^2 \right) x &= 0, \\ \ddot{y} + 2\Omega_0\dot{x} + \omega_A^2 y &= 0, \end{aligned} \quad (5)$$

where the Alfvén frequency, ω_A , measures the intensity of the magnetic tension force. With $\omega_A = 0$ and Keplerian rotation $\Omega(R) \sim R^{-3/2}$ the equations (5) are reduced to the Hill-Clohessy-Wiltshire ones [31, 32] that describe in particular the relative motion of two satellites.

Writing down the characteristic equation of system (5) and taking into account that at the onset of standard MRI with only an axial magnetic field applied (which is a non-oscillatory instability) the critical eigenvalue is vanishing [33], we get the instability threshold (see also [16])

$$\text{Ro} := \frac{1}{2} \frac{R}{\Omega} \frac{d\Omega}{dR} = -\frac{\omega_A^2}{4\Omega_0^2}, \quad (6)$$

where Ro is the Rossby number (evaluated at $R = R_0$ in (6)) that indicates the deviation of the rotating shear flow from the solid body rotation, $\text{Ro} = 0$. The latter is the threshold resulting from the sufficient stability criterion of Velikhov-Chandrasekhar ($\text{Ro} > 0$). The actual threshold of MRI given by equation (6) depends on the magnetic field strength through ω_A and therefore it coincides with the criterion (3) in the limit $\omega_A = 0$ which deviates from the non-magnetic value $\text{Ro} = -1$ following from the Rayleigh criterion (1). This non-uniqueness of the critical Rossby number in the non-magnetic limit is another manifestation of the Velikhov-Chandrasekhar paradox.

In contrast to the non-magnetic Couette-Taylor case, the theory of MRI was ahead of laboratory experiments. First interesting experimental results were obtained only in 2004 in a spherical Couette flow of liquid sodium [34]. In this experiment, the authors observed correlated modes of velocity and magnetic field perturbation in parameter regions which are quite typical for MRI. However, the background state in this spherical Couette experiment was already fully turbulent, so that the original goal to show the basic destabilizing effect of a magnetic field was not met. Recent works [35, 36] have also shown

that the observed effects might be alternatively explained in terms of two different sorts of non-axisymmetric magnetic instabilities in spherical Couette flow.

At Princeton University, work is going on to identify MRI in a CT-experiment with liquid gallium, and first encouraging results, including the observation of nonaxisymmetric magneto-Coriolis (MC) waves, have been recently reported [37,38]. The Princeton facility had been designed to investigate the standard version of MRI (SMRI) with only a vertical magnetic field being applied. SMRI is known to work only with magnetic Reynolds numbers (R_m) in the order of 1 or larger. R_m is proportional to the hydrodynamic Reynolds number according to $R_m = PmRe$, where Pm is the magnetic Prandtl number. For liquid metals Pm is typically in the range $10^{-6} - 10^{-5}$. Therefore, in order to achieve $R_m \sim 1$, we need $Re = 10^5 - 10^6$, and wall-constrained flows (in contrast to wall-free Keplerian flows) with such high Re are usually turbulent, whatever the linear stability analysis might tell [39]. This is the point which makes SMRI experiments, and their interpretation, so cumbersome [40].

This situation changed drastically when Hollerbach and Rüdiger considered the effect of adding an azimuthal magnetic field to the axial one [41]. Indeed, it was shown [41,42] that the resulting helical MRI (HMRI), as we now call it, is then possible at far smaller Reynolds numbers and magnetic field amplitudes than SMRI, making HMRI an ideal playground for liquid metal experiments.

First experimental evidence for HMRI was obtained in 2006 at the liquid metal facility PROMISE (Potsdam ROssendorf Magnetic InStability Experiment) which is basically a CT-cell made of concentric rotating copper walls, filled with GaInSn (a eutectic which is liquid at room temperatures). In [43,44,45] it was shown that the HMRI traveling wave appears only in the predicted finite window of the magnetic field intensity, with a frequency of the traveling wave that was in rather good accordance with numerical simulations. Some disturbing effects of this early version (PROMISE 1), connected with the recirculating radial jet at midheight of the cylinder, were overcome in the follow-up PROMISE 2 experiment by splitting the axial end caps to suppress the Ekman pumping [46,47]. By comparing experimental and numerical (based on [48]) results for a wide variety of parameter dependencies, it was possible to identify the observed instability as an absolute one, distinguishing it clearly from a noise triggered convective instability as speculated on in [49].

Despite SMRI being a non-oscillatory instability and HMRI being an oscillatory one, there is a continuous and monotonic transition between them when Re and the magnetic field strength are increased simultaneously [41,50]. This is all the more remarkable in that HMRI has been identified with the destabilization of an inertial wave in apparent contrast to SMRI that is a destabilized slow Magneto-Coriolis wave [51,52,53,54]. The transition from SMRI to HMRI, which are characterized by substantially different scaling laws, involves the origination of a spectral exceptional point [55] and a transfer of instability between the modes [54].

It is remarkable, too, that even in the limit of vanishing electrical conductivity ($Pm \rightarrow 0$), the helical magnetic field is able to trigger an instability

although the instantaneous growth of the energy of any perturbation must be smaller than in the field-free case—the *paradox of inductionless HMRI* [53]. In this inductionless case, however, the local WKB analysis in the small-gap approximation prohibits helical magnetorotational instability when Ro exceeds the Liu limit of $2 - 2\sqrt{2} \simeq -0.828$ [51]. Thus the inductionless HMRI works only for comparably steep rotation profiles (i.e., slightly above the Rayleigh line of $Ro = -1$) and disappears for profiles as flat as the Keplerian one with $Ro = -0.75$, see also [52, 50]. This behaviour has been experimentally confirmed in the PROMISE experiment [25].

Applicability of HMRI to higher Rossby numbers is sensitive also to electrical boundary conditions [56]. In addition to this, HMRI at the Rossby numbers slightly above the Liu limit was observed already in the WKB approximation at small but finite Pm in [54].

The ultimate upper limit of the critical Ro in this case is an intriguing question, in particular because of new arguments that arose recently from investigations of the saturation regime of MRI. For the case of small magnetic Prandtl numbers (as they are typical for the outer parts of accretion disks [57, 58]), Umurhan [59] speculated about a saturated rotation profile with regions of reduced shear, sandwiched by regions of strengthened shear. For those latter regions with steeper than Keplerian profiles, HMRI could indeed become of significant relevance.

Despite a more than a century-long history, hydrodynamic and hydromagnetic stability of rotating shear flows remains a vibrant area of research, full of intriguing paradoxes and mathematical, computational, and experimental challenges. Below extending the recent works of the authors [54, 60] we present a viewpoint that relates some of the mentioned effects to singularity theory—an approach that had already proven its efficiency in the field of dissipation-induced instabilities [61, 62, 63, 64, 65, 66, 67, 68, 69, 70, 71, 72].

2 Mathematical setting

The standard set of non-linear equations of dissipative incompressible magnetohydrodynamics [52, 50, 54] consists of the Navier-Stokes equation for the fluid velocity \mathbf{u}

$$\frac{\partial \mathbf{u}}{\partial t} + (\mathbf{u} \cdot \nabla) \mathbf{u} = -\frac{1}{\rho} \nabla \left(p + \frac{\mathbf{B}^2}{2\mu_0} \right) + \frac{1}{\mu_0 \rho} (\mathbf{B} \cdot \nabla) \mathbf{B} + \nu \nabla^2 \mathbf{u}, \quad (7)$$

and of the induction equation for the magnetic field \mathbf{B}

$$\frac{\partial \mathbf{B}}{\partial t} = \nabla \times (\mathbf{u} \times \mathbf{B}) + \eta \nabla^2 \mathbf{B}, \quad (8)$$

where p is the pressure, $\rho = \text{const}$ the density, $\nu = \text{const}$ the kinematic viscosity, $\eta = (\mu_0 \sigma)^{-1}$ the magnetic diffusivity, σ the conductivity of the fluid, and μ_0 the magnetic permeability of free space. Additionally, the mass

continuity equation for incompressible flows and the solenoidal condition for the magnetic induction yield

$$\nabla \cdot \mathbf{u} = 0, \quad \nabla \cdot \mathbf{B} = 0. \quad (9)$$

We consider the rotational fluid flow in the gap between the radii R_1 and $R_2 > R_1$, with an imposed magnetic field sustained by currents external to the fluid. Introducing the cylindrical coordinates (R, ϕ, z) we consider the stability of a steady-state background liquid flow with the angular velocity profile $\Omega(R)$ in a helical background magnetic field (a magnetized CT-flow)

$$\mathbf{u}_0 = R \Omega(R) \mathbf{e}_\phi, \quad p = p_0(R), \quad \mathbf{B}_0 = B_\phi^0(R) \mathbf{e}_\phi + B_z^0 \mathbf{e}_z, \quad (10)$$

with the azimuthal component

$$B_\phi^0(R) = \frac{\mu_0 I}{2\pi R}, \quad (11)$$

which can be thought as being produced by an axial current I . The angular velocity profile of the background CT-flow is [25]

$$\Omega(R) = \frac{\Omega_1 R_1^2 - \Omega_2 R_2^2}{R_1^2 - R_2^2} + \frac{1}{R^2} \frac{(\Omega_2 - \Omega_1) R_1^2 R_2^2}{R_1^2 - R_2^2}. \quad (12)$$

The centrifugal acceleration of the background flow (12) is compensated by the pressure gradient

$$\frac{1}{\rho} \frac{\partial p_0}{\partial R} = R \Omega^2. \quad (13)$$

2.1 Linearization with respect to axisymmetric perturbations

Throughout the paper we will restrict our interest to axisymmetric perturbations $\mathbf{u}' = \mathbf{u}'(R, z)$, $\mathbf{B}' = \mathbf{B}'(R, z)$, and $p' = p'(R, z)$ about the stationary solution (10)-(12). Non-axisymmetric perturbations become important for the so-called azimuthal MRI (AMRI) and the Tayler instability [73, 74].

With the notation

$$\partial_t = \frac{\partial}{\partial t}, \quad \partial_R = \frac{\partial}{\partial R}, \quad \partial_z = \frac{\partial}{\partial z}, \quad \partial_R^\dagger = \partial_R + \frac{1}{R}, \quad D = \partial_R \partial_R^\dagger + \partial_z^2 \quad (14)$$

we write the linearized equations that couple u'_R , u'_ϕ and B'_R , B'_ϕ [54]

$$\partial_t \tilde{E} \xi' = \tilde{H} \xi', \quad (15)$$

where $\xi' = (u'_R, u'_\phi, B'_R, B'_\phi)^T$, and

$$\tilde{E} = \begin{pmatrix} D & 0 & 0 & 0 \\ 0 & 1 & 0 & 0 \\ 0 & 0 & 1 & 0 \\ 0 & 0 & 0 & 1 \end{pmatrix}, \quad \tilde{H} = \begin{pmatrix} \nu D^2 & 2\Omega \partial_z^2 & \frac{B_z^0}{\mu_0 \rho} D \partial_z & -\frac{2B_\phi^0}{\mu_0 \rho R} \partial_z^2 \\ -2\Omega(1 + \text{Ro}) & \nu D & 0 & \frac{B_z^0}{\mu_0 \rho} \partial_z \\ B_z^0 \partial_z & 0 & \eta D & 0 \\ \frac{2B_\phi^0}{R} & B_z^0 \partial_z & 2\Omega \text{Ro} & \eta D \end{pmatrix}. \quad (16)$$

The resulting multiparameter family of operator matrices equipped with boundary conditions can be investigated by numerical or perturbative [75] methods. In the following we use the local WKB approximation.

2.2 Local WKB approximation

We expand all the background quantities in Taylor series around a fiducial point (R_0, z_0) and retain only the zeroth order in terms of the local coordinates $\tilde{R} = R - R_0$ and $\tilde{z} = z - z_0$ to obtain the operator matrix equation

$$\partial_t \tilde{E}_0 \xi' = \tilde{H}_0 \xi' \quad (17)$$

with

$$\tilde{E}_0 = \begin{pmatrix} D_0 & 0 & 0 & 0 \\ 0 & 1 & 0 & 0 \\ 0 & 0 & 1 & 0 \\ 0 & 0 & 0 & 1 \end{pmatrix}, \quad \tilde{H}_0 = \begin{pmatrix} \nu(D_0)^2 & 2\Omega_0 \partial_{\tilde{z}}^2 & \frac{B_z^0}{\mu_0 \rho} D_0 \partial_{\tilde{z}} & -\frac{2B_\phi^0}{\mu_0 \rho R_0} \partial_{\tilde{z}}^2 \\ -2\Omega_0(1 + \text{Ro}) & \nu D_0 & 0 & \frac{B_z^0}{\mu_0 \rho} \partial_{\tilde{z}} \\ B_z^0 \partial_{\tilde{z}} & 0 & \eta D_0 & 0 \\ \frac{2B_\phi^0}{R_0} & B_z^0 \partial_{\tilde{z}} & 2\Omega_0 \text{Ro} & \eta D_0 \end{pmatrix}, \quad (18)$$

where

$$\Omega_0 = \Omega(R_0), \quad B_\phi^0 = B_\phi^0(R_0), \quad D_0 = \partial_{\tilde{R}}^2 + \partial_{\tilde{z}}^2 + \frac{\partial_{\tilde{R}}}{R_0} - \frac{1}{R_0^2}. \quad (19)$$

Equation (17) is a linear PDE with the constant coefficients in the local variables (\tilde{R}, \tilde{z}) for the perturbed quantities ξ' , which is valid as long as \tilde{R} and \tilde{z} are small in comparison with the characteristic radial and vertical length scales (the so-called narrow-gap approximation [76]). A plane wave solution to the equation (17) is

$$\xi' = \hat{\xi} \exp(ik_R \tilde{R} + ik_z \tilde{z}), \quad \hat{\xi} = \tilde{\xi} \exp(\gamma t), \quad (20)$$

where $\tilde{\xi}$ is a vector of constant coefficients and $\hat{\xi} = (\hat{u}_R, \hat{u}_\phi, \hat{B}_R, \hat{B}_\phi)^T$.

In the WKB approximation we restrict the analysis to the short-wave modes with the wave numbers satisfying $k_R \gg \frac{1}{R_0}$ which allows us to neglect the terms $\frac{ik_R}{R_0} - \frac{1}{R_0^2}$ in (17). In view of this, substituting (20) into equation (17), yields the leading order WKB equations that describe the onset of instability of a CT-flow with a helical external magnetic field

$$\dot{\xi} = H \xi, \quad H = \begin{pmatrix} -\omega_\nu & 2\Omega_0 \alpha^2 & i\omega_A & -2\omega_{A_\phi} \alpha^2 \\ -2\Omega_0(1 + \text{Ro}) & -\omega_\nu & 0 & i\omega_A \\ i\omega_A & 0 & -\omega_\eta & 0 \\ 2\omega_{A_\phi} & i\omega_A & 2\Omega_0 \text{Ro} & -\omega_\eta \end{pmatrix}, \quad (21)$$

where $\xi = (\hat{u}_R, \hat{u}_\phi, \hat{B}_R(\mu_0 \rho)^{-1/2}, \hat{B}_\phi(\mu_0 \rho)^{-1/2})^T$, $\alpha = k_z/k$, the total wave number is defined through $k^2 = k_z^2 + k_R^2$, $\omega_\nu = \nu k^2$ and $\omega_\eta = \eta k^2$ are the

viscous and resistive frequencies, and the Alfvén frequencies of the axial and azimuthal magnetic field components are

$$\omega_A^2 = \frac{k_z^2 (B_z^0)^2}{\mu_0 \rho}, \quad \omega_{A_\phi}^2 = \frac{(B_\phi^0)^2}{\mu_0 \rho R_0^2}, \quad (22)$$

respectively [54].

3 Stability analysis

The stability of solutions to the equation (21) is determined by the roots γ of the dispersion equation

$$P(\gamma) = \gamma^4 + a_1 \gamma^3 + a_2 \gamma^2 + (a_3 + ib_3) \gamma + a_4 + ib_4 = 0, \quad (23)$$

where $P(\gamma) = \det(H - \gamma E)$ and E is the unit matrix. We write the coefficients of the complex polynomial (23) in the form [50, 51, 52, 54]

$$\begin{aligned} a_1 &= 2(\omega_\nu + \omega_\eta), \\ a_2 &= (\omega_\nu + \omega_\eta)^2 + 2(\omega_A^2 + \omega_\nu \omega_\eta) + 4\alpha^2 \Omega_0^2 (1 + \text{Ro}) + 4\alpha^2 \omega_{A_\phi}^2, \\ a_3 &= 2(\omega_\eta + \omega_\nu)(\omega_A^2 + \omega_\eta \omega_\nu) + 8\alpha^2 \Omega_0^2 (1 + \text{Ro}) \omega_\eta + 4\alpha^2 (\omega_\eta + \omega_\nu) \omega_{A_\phi}^2, \\ a_4 &= (\omega_A^2 + \omega_\nu \omega_\eta)^2 - 4\alpha^2 \omega_A^2 \Omega_0^2 + 4\alpha^2 \Omega_0^2 (1 + \text{Ro}) (\omega_A^2 + \omega_\eta^2) + 4\alpha^2 \omega_\nu \omega_\eta \omega_{A_\phi}^2, \\ b_3 &= -8\alpha^2 \Omega_0 \omega_A \omega_{A_\phi}, \\ b_4 &= -4\alpha^2 \Omega_0 \omega_A \omega_{A_\phi} (2\omega_\eta + \omega_\nu) - 4\alpha^2 \Omega_0 (1 + \text{Ro}) \omega_A \omega_{A_\phi} (\omega_\eta - \omega_\nu). \end{aligned} \quad (24)$$

With $\omega_{A_\phi} = 0$ the coefficients b_3 and b_4 vanish while the others simplify. Composing the Hurwitz matrix of the resulting real polynomial, we write the Lienard and Chipart criterion of asymptotic stability [77]

$$a_4 > 0, \quad a_2 > 0, \quad h_1 = a_1 > 0, \quad h_3 = a_1 a_2 a_3 - a_1^2 a_4 - a_3^2 > 0. \quad (25)$$

Under the physical assumption that $\omega_\nu \geq 0$ and $\omega_\eta \geq 0$, the last two inequalities are automatically satisfied, because

$$\begin{aligned} h_3 &= 4\omega_A^2 (\omega_\eta + \omega_\nu)^2 ((\omega_\eta + \omega_\nu)^2 + 4\Omega_0^2 \alpha^2) \\ &\quad + 4\omega_\eta \omega_\nu ((\omega_\eta + \omega_\nu)^2 + 4\Omega_0^2 \alpha^2 (1 + \text{Ro}))^2 > 0. \end{aligned} \quad (26)$$

On the other hand, condition $a_4 > 0$ implies that

$$\text{Ro} > \text{Ro}_c := -\frac{(\omega_A^2 + \omega_\nu \omega_\eta)^2 + 4\Omega_0^2 \omega_\eta^2 \alpha^2}{4\Omega_0^2 \alpha^2 (\omega_A^2 + \omega_\eta^2)} > -1 - \frac{\omega_\nu^2}{4\alpha^2 \Omega_0^2}, \quad (27)$$

which yields $a_2 > 0$. Therefore, the four stability conditions (25) are reduced to the only (27) that yields the critical Rossby number (Ro_c) of SMRI (above which the flow is stable).

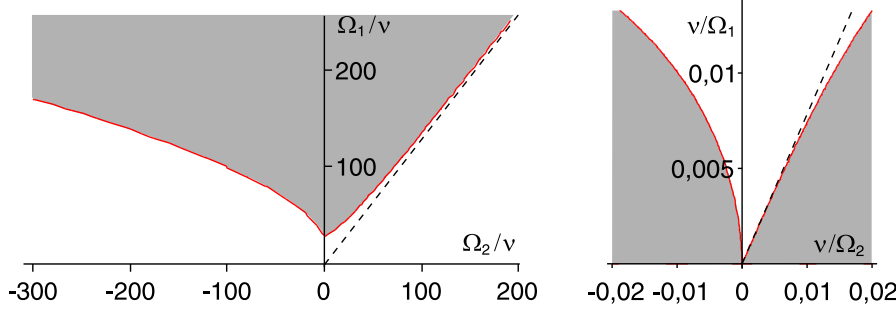


Fig. 4 Stability diagrams according to the WKB thresholds (35) and (36) with centrifugal instability shown in grey and stability in white calculated for the Taylor values $R_1 = 3.55$ cm and $R_2 = 4.035$ cm: (left) in $(\Omega_2/\nu, \Omega_1/\nu)$ -plane [78] and (right) in $(\nu/\Omega_2, \nu/\Omega_1)$ -plane; dashed line is the Rayleigh threshold.

Alternatively, this threshold follows from equations (21) that can be rewritten as a non-conservative gyroscopic system

$$\ddot{u} + (D + \Omega_0(1 + \alpha^2)J)\dot{u} + (N + K)u = 0, \quad (28)$$

where $u = (\hat{u}_R, \hat{u}_\phi)^T$, $N = \Omega_0(\omega_\eta(1 + \alpha^2) + \text{Ro}(\omega_\eta - \omega_\nu))J$,

$$K = \begin{pmatrix} \omega_A^2 + \omega_\nu\omega_\eta & k_{12} \\ k_{12} & \omega_A^2 + \omega_\nu\omega_\eta + 4\alpha^2\Omega_0^2\text{Ro} \end{pmatrix} \quad (29)$$

with $k_{12} = \Omega_0(\omega_\eta(1 - \alpha^2) + \text{Ro}(\omega_\eta - \omega_\nu))$, and

$$J = \begin{pmatrix} 0 & -1 \\ 1 & 0 \end{pmatrix}, \quad D = \begin{pmatrix} \omega_\nu + \omega_\eta & \Omega_0(1 - \alpha^2) \\ \Omega_0(1 - \alpha^2) & \omega_\nu + \omega_\eta \end{pmatrix}. \quad (30)$$

For $\alpha = 1$, $\omega_\nu = 0$, and $\omega_\eta = 0$, Eq. (28) is similar to the model (5) and has the same dispersion equation.

Stable perturbations have $\Re \gamma \leq 0$ provided that γ with $\Re \gamma = 0$ is a semi-simple eigenvalue of the eigenvalue problem corresponding to (28). The growing solutions of SMRI are non-oscillatory with $\Im \gamma = 0$. Therefore, $\gamma = 0$ implies that $\det(N + K) = 0$ at the threshold of SMRI which gives the critical Rossby number, Ro_c .

3.1 Non-magnetic Couette-Taylor flow

In the absence of the magnetic field $\omega_A = 0$ and

$$\text{Ro}_c = -1 - \frac{\omega_\nu^2}{4\alpha^2\Omega_0^2}, \quad (31)$$

which exactly reproduces the result of Eckhardt and Yao obtained by means of the geometrical optics stability analysis [78].

Following [78], we write the condition for centrifugal instability as

$$\text{Ro}_c < -1 - \frac{\nu^2}{4\Omega_0^2} \frac{(1 + k_z^2/k_R^2)^3}{k_z^2/k_R^2} k_R^4 \leq -1 - \frac{\nu^2}{4\Omega_0^2} \frac{27}{4} k_R^4. \quad (32)$$

Using the definition of the Rossby number (6) and the profile of angular velocity (12) in the inequality (32), we transform it into

$$\frac{\Omega_1 R_1^2 - \Omega_2 R_2^2}{R_1^2 - R_2^2} \Omega(R_1) \leq \frac{\Omega_1 R_1^2 - \Omega_2 R_2^2}{R_1^2 - R_2^2} \Omega(R_0) \leq -\nu^2 \frac{27}{16} k_R^4, \quad (33)$$

where $\Omega(R_1) = \Omega_1$. Restricting the radial wave number from below further by $|k_R| > \pi/(R_2 - R_1)$ in case of co-rotating cylinders ($\Omega_2 \geq 0$) and by $|k_R| > \pi/(R_c - R_1)$ in case of counter-rotation ($\Omega_2 < 0$), where R_c is the radius at which $\Omega(R)$ changes its sign, see [78]

$$R_c = \sqrt{\frac{\Omega_1 - \Omega_2}{\Omega_1 R_1^2/R_2^2 - \Omega_2}} R_1, \quad (34)$$

and taking into account the narrow-gap approximation, equivalent to the condition $(R_2 - R_1)/R_1 \ll 1$, we derive the WKB approximations to the Taylor instability domain for $\Omega_2 \geq 0$

$$\Omega_2 < \frac{R_1^2}{R_2^2} \left(1 - \frac{\Omega_c^2}{\Omega_1^2}\right) \Omega_1 \quad (35)$$

and for $\Omega_2 < 0$

$$\Omega_2 > \frac{R_1^2}{R_2^2} \left(1 - \frac{\Omega_1^2}{\Omega_c^2}\right) \Omega_1, \quad (36)$$

where

$$\Omega_c = \nu \sqrt{\frac{27\pi^4}{8R_1(R_2 - R_1)^3}}. \quad (37)$$

In Fig. 4(left) we see that the local WKB approximation (31) qualitatively and quantitatively correctly reproduces the Taylor's stability diagram that was obtained from the analysis of the global boundary eigenvalue problem. Since the modern experiments intending to observe SMRI require very high Reynolds numbers [34, 39, 40], it is instructive to redraw this stability diagram in the $(\nu/\Omega_2, \nu/\Omega_1)$ -plane, Fig. 4(right). In this plane the stability domain shown in white in Fig. 4(right) has a self-intersection singularity at the origin, which at least illustrates the recent experimental evidence that at high Reynolds numbers the ratio Ω_1/Ω_2 is 'the dominant control parameter for rotating shear flows' [39]. The existence of such a singularity that causes high sensitivity of the instability threshold to the variation of the parameters might be a reason for a controversy in the experiments [34, 39] that indicate both laminar and turbulent states of the CT-flow at high Reynolds numbers [40].

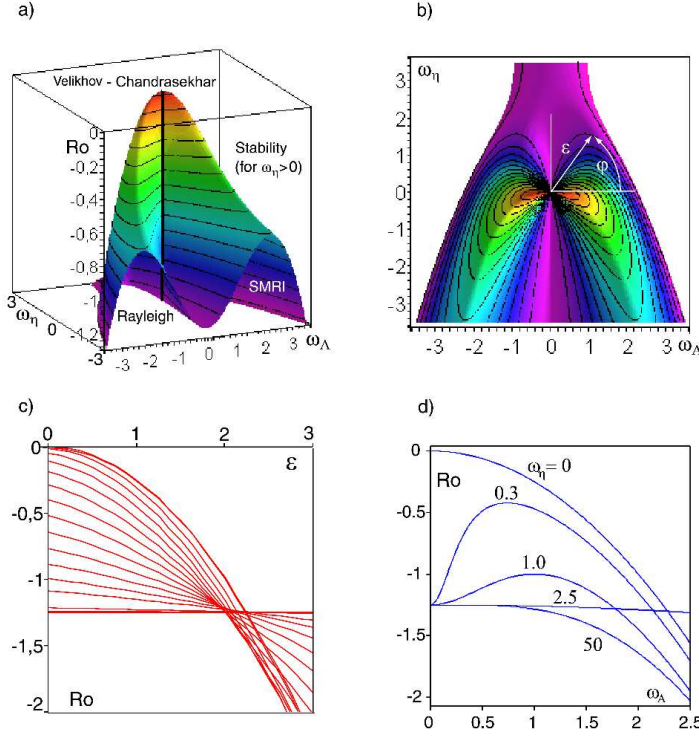


Fig. 5 (a) The critical Rossby number of SMRI as a function of $\omega_A \sim \text{LuPm}^{-1}$ and $\omega_\eta \sim \text{Pm}^{-1}$ for $\omega_\nu = 1$, $\alpha = 1$, $\Omega_0 = 1$, i.e. for $\text{Re} = 1$. (b) Top view of the surface. (c) Cross-sections of the surface along the rays specified by the Lundquist number, or, equivalently, by the angle φ that varies from 0 to 1.5 through the equal intervals $\Delta\varphi = 0.1$; the horizontal line corresponds to $\varphi = \pi/2$. (d) Transition between the case of low (Velikhov 1959) and high (Chandrasekhar 1953) resistivity.

3.2 Velikhov-Chandrasekhar paradox in standard MRI

The Velikhov-Chandrasekhar paradox occurs at infinite $\text{Pm} = \omega_\nu \omega_\eta^{-1}$ and means that in the ideal MHD case ($\omega_\eta = 0$, $\omega_\nu = 0$) the limit $\omega_A \rightarrow 0$ yields Velikhov's value $\text{Ro}_c = 0$ as the instability threshold rather than Rayleigh's limit $\text{Ro}_c = -1$ of the non-magnetic case ($\omega_A = 0$, $\omega_\nu = 0$).

With $\omega_A = \varepsilon \cos \varphi$ and $\omega_\eta = \varepsilon \sin \varphi$ in (27), we obtain

$$\text{Ro}_c = -\frac{(\varepsilon \cos^2 \varphi + \omega_\nu \sin \varphi)^2 + 4\alpha^2 \Omega_0^2 \sin^2 \varphi}{4\alpha^2 \Omega_0^2}, \quad (38)$$

which for $\varepsilon \rightarrow 0$ reduces to

$$\text{Ro}_c = -\left(1 + \frac{1}{4\text{Re}^2}\right) \sin^2 \varphi = -\frac{1 + (2\text{Re})^{-2}}{1 + \text{Lu}^2}, \quad (39)$$

where $\text{Re} = \Omega_0 \alpha \omega_\nu^{-1}$ and $\text{Lu} = \omega_A \omega_\eta^{-1}$ are the Reynolds and the Lundquist numbers, respectively. Introducing the new parameter $\text{Ro}' = (1 + 4\text{Re}^2(1 + 2\text{Ro}))(1 + 4\text{Re}^2)^{-1}$ we find that in the $(\omega_A, \omega_\eta, \text{Ro}')$ -space Eq. (39) defines a so-called *ruled surface* $(\varepsilon, \varphi) \mapsto (\varepsilon \cos \varphi, \varepsilon \sin \varphi, \cos n\varphi)$ with $n = 2$, which is a canonical equation for the Plücker conoid of degree $n = 2$ [79, 80]. The surface according to Eq. (27) tends to the Plücker conoid when $\varepsilon = \sqrt{\omega_A^2 + \omega_\eta^2} \rightarrow 0$.

This surface is shown in the $(\omega_A, \omega_\eta, \text{Ro})$ -space in Fig. 5(a) and in projection to the (ω_A, ω_η) -plane in Fig. 5(b) for $\text{Re} = 1$. For each α , ω_ν , and Ω_0 it has the same Plücker conoid singularity, i.e. an interval of self-intersection along the Ro -axis and two Whitney umbrella singular points at its ends. This singular structure implies non-uniqueness for the critical Rossby number when simultaneously $\omega_A = 0$ and $\omega_\eta = 0$.

Indeed, for a given Lu , tending the magnetic field to zero along a ray $\omega_A = \omega_\eta \text{Lu}$ in the (ω_A, ω_η) -plane results in a value of the Rossby number specified by Eq. (39), see Fig. 5(c). The limit value of the critical Rossby number oscillates between the ideal MHD value $\text{Ro}_c = 0$ for $\text{Lu} = \infty$ ($\varphi = 0$) and the non-magnetic (Taylor) value $\text{Ro}_c = -1 - (2\text{Re})^{-2}$ for $\text{Lu} = 0$ ($\varphi = \pi/2$), which resolves the Velikhov-Chandrasekhar paradox.

Physically, the Lundquist number determines the ‘lifetime’ of the magnetic field line that is frozen into the fluid. In the ideal MHD case $\text{Lu} = \infty$ means that the field does not diffuse from the fluid. At the lower values of Lu resistivity destroys the magnetic tension effect which prevents Ro from reaching the solid body rotation value in the limit of vanishing magnetic field.

Fig. 5(d) demonstrates transition between the cases of high conductivity (Velikhov 1959) and of low conductivity (Chandrasekhar 1953) separated by the threshold $\omega_\eta = (\omega_\nu^2 + 4\Omega_0^2 \alpha^2)(2\omega_\nu)^{-1}$. In the latter case the axial magnetic field stabilizes the hydrodynamically unstable CT-flow. Fig. 5(d) also illustrates the conclusions of Acheson and Hide that in the presence of small but finite resistivity in the limit of vanishing ω_A “the stability or otherwise of the system will then be decided essentially by Rayleigh’s criterion” [21].

What eigenvalue behavior corresponds to the singular threshold of SMRI? In the absence of the magnetic field the roots of the dispersion equation (23) are exactly

$$\gamma_{1,2} = -\omega_\nu \pm i2\alpha\Omega_0\sqrt{\text{Ro} + 1}, \quad \gamma_{3,4} = -\omega_\eta. \quad (40)$$

The first two roots bifurcate and one of them becomes positive at the critical Rossby number given by equation (31), see Fig. 6(a,b,e). The blue curves there represent the inertial waves whose interaction yields the centrifugal instability in the inviscid case [81]. The Rayleigh line is thus characterized by the double zero eigenvalue with the Jordan block. Viscosity shifts this doublet to the left part of the complex plane [82]. This scenario corresponds to the lower Whitney umbrella singularity on the SMRI threshold surface shown in Fig. 5(a).

With $\omega_A \neq 0$ the merging of the inertial waves becomes imperfect, see Fig. 6(c,d), while the formerly damped roots $\gamma_{3,4}$ experience a bifurcation at the Rossby number that is close to the Velikhov-Chandrasekhar value. In Fig. 6(d) the red branches correspond to the slow Magneto-Coriolis (MC)

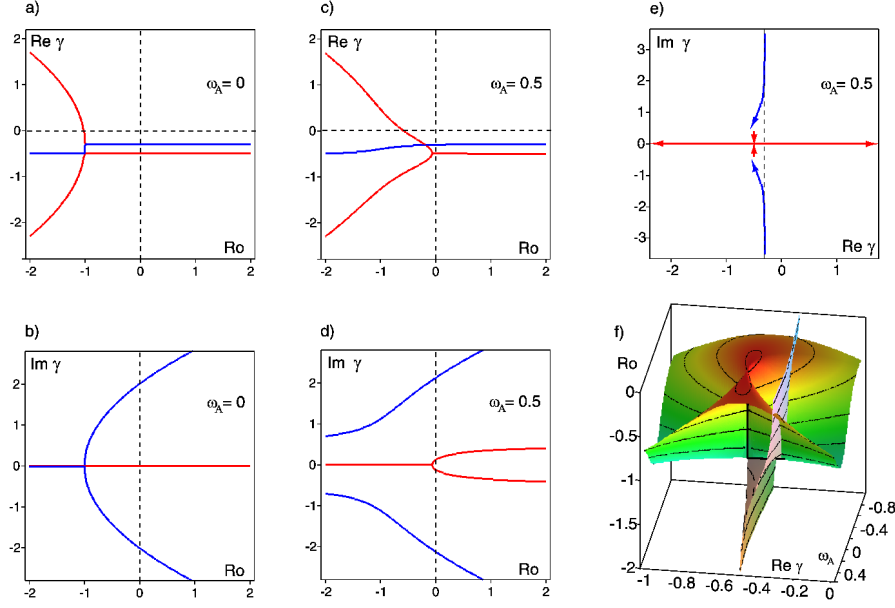


Fig. 6 Growth rates and frequencies of the perturbation for $\Omega_0 = 1$, $\alpha = 1$, $\omega_\nu = 0.3$, $\omega_\eta = 0.5$ and (a,b) $\omega_A = 0$ and (c,d,e) $\omega_A = 0.5$; (f) growth rates surfaces in the $(\Re \gamma, \omega_A, Ro)$ -space.

waves while the blue ones — to the fast Magneto-Coriolis waves. Bifurcation of the slow MC-waves precedes the onset of SMRI (equation (27)) with the decrease of Ro . In the absence of viscosity and resistivity the roots of the dispersion equation (23) corresponding to slow- and fast MC-waves are exactly

$$\gamma^2 = -2\Omega_0^2\alpha^2(1 + Ro) - \omega_A^2 \pm 2\Omega_0\alpha\sqrt{\Omega_0^2\alpha^2(1 + Ro)^2 + \omega_A^2}. \quad (41)$$

The corresponding double zero eigenvalue at $\omega_A = 0$ and $Ro = 0$ is related to the upper Whitney umbrella singularity at the threshold surface of SMRI in Fig. 5(a).

Transition between these two bifurcations happens in the presence of resistivity and viscosity and is described by means of the slices of two singular eigenvalue surfaces shown in Fig. 6(f). The surface corresponding to the roots $\gamma_{1,2}$ is locally equivalent to the Plücker conoid of degree $n = 2$ while that of the roots $\gamma_{3,4}$ is locally equivalent to the Plücker conoid of degree $n = 1$ [79].

3.3 Paradox of inductionless helical magnetorotational instability

Now we turn over to the paradox of inductionless HMRI which is related to a similar geometric singularity as discussed above.

After scaling the spectral parameter as $\gamma = \lambda\sqrt{\omega_\nu\omega_\eta}$, we express the appropriately normalized coefficients (24) by means of the dimensionless Rossby

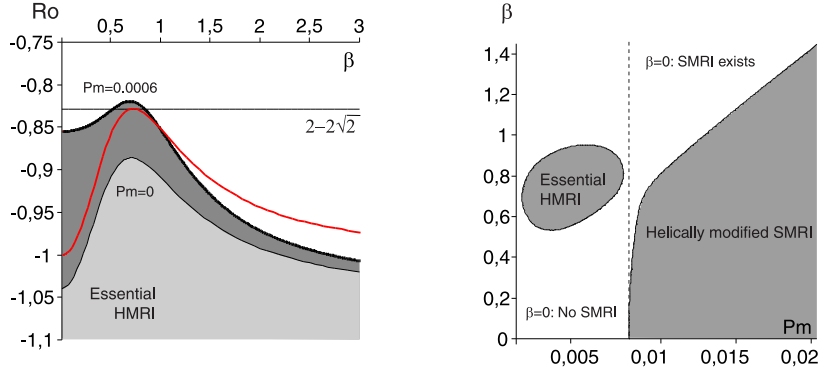


Fig. 7 (left) In the inductionless limit $Pm = 0$ the instability domain (light grey, shown for $Ha = 19$ and $Re = 900$) is always under the majorating red curve given by Eq. (45) that touches the Liu limit $Ro = 2 - 2\sqrt{2}$ at $\beta = \sqrt{2}/2$; for $Pm \neq 0$ however this is no longer true and the instability domain (dark grey, shown for $Ha = 19$ and $Re = 900$) can partly lie above the Liu limit. (right) HMRI island (shown for $Ha = 5$, $Re = 100$, and $Ro = -0.85$) in the (Pm, β) -plane exists at such low Pm at $\beta \neq 0$ where SMRI at $\beta = 0$ doesn't [54].

number (Ro), magnetic Prandtl number (Pm), helicity parameter $\beta = \alpha \omega_{A_\phi} \omega_A^{-1}$ of the external magnetic field, Hartmann ($Ha = Lu Pm^{-1/2}$), and Reynolds (Re) numbers. Additional transformations yield the coefficients of the dispersion equation $P(\lambda) = 0$

$$\begin{aligned}
 a_1 &= 2(1 + Pm^{-1})\sqrt{Pm}, \\
 a_2 &= 2(1 + (1 + 2\beta^2)Ha^2) + 4Re^2(1 + Ro)Pm + a_1^2/4, \\
 a_3 &= a_1(1 + (1 + 2\beta^2)Ha^2) + 8Re^2(1 + Ro)\sqrt{Pm}, \\
 a_4 &= (1 + Ha^2)^2 + 4\beta^2Ha^2 + 4Re^2(1 + Ro(PmHa^2 + 1)), \\
 b_3 &= -8\beta Ha^2 Re \sqrt{Pm}, \quad b_4 = b_3(1 + (1 - Pm)Ro/2)/\sqrt{Pm}. \quad (42)
 \end{aligned}$$

The analogue of the Routh-Hurwitz conditions for the complex polynomials—the Bilharz criterion [83]—requires positiveness of all diagonal even-ordered minors of the so-called Bilharz matrix composed of the coefficients (42)

$$\begin{aligned}
 m_1 &= a_3a_4 + b_3b_4 > 0, \quad m_2 = (a_2a_3 - a_1a_4)m_1 - a_2^2b_4^2 > 0, \\
 m_3 &= (a_1a_2 - a_3)m_2 - (a_1^2a_4a_2 + (a_1b_3 - b_4)^2)m_1 \\
 &\quad + a_1a_4(b_4a_2(2b_4 - a_1b_3) + a_1^2a_4^2) > 0, \\
 m_4 &= a_1m_3 - a_1a_3m_2 + (a_3^3 + a_1^2b_4b_3 - 2a_1b_4^2)m_1 \\
 &\quad + a_1b_4^2a_4(a_1a_2 - a_3) - b_4^2a_3^2a_2 + b_4^4 > 0. \quad (43)
 \end{aligned}$$

When the last of the stability conditions (43) is fulfilled, the remaining inequalities are satisfied automatically [54]. Therefore, the threshold of HMRI is defined by the equation $m_4(\beta, Re, Ha, Pm, Ro) = 0$. For $\beta = 0$ the dispersion equation and thus the threshold for HMRI reduce to that of SMRI [54].

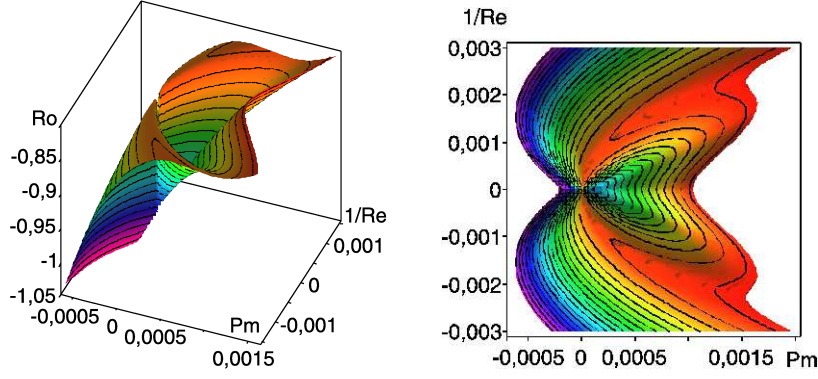


Fig. 8 Instability threshold in the presence of the helical magnetic field for $Ha = 15$ and $\beta = 0.7$ in the (Pm, Re^{-1}, Ro) -space and in projection to the (Pm, Re^{-1}) -plane.

In the inductionless limit $Pm \rightarrow 0$ the critical Rossby number for the onset of HMRI follows from the equation $m_4 = 0$ in the explicit form

$$Ro = \frac{(1+Ha^2)^2 + 4\beta^2 Ha^2(1+\beta^2 Ha^2)}{2Ha^4 \beta^2} - \frac{2\beta^2 Ha^2 + Ha^2 + 1}{2Ha^4 \beta^2} \times \sqrt{(1+Ha^2)^2 + 4\beta^2 Ha^2(1+\beta^2 Ha^2) + \frac{Ha^4 \beta^2}{Re^2} ((1+Ha^2)^2 + 4\beta^2 Ha^2)}. \quad (44)$$

In the limit $Re \rightarrow \infty$ and $Ha \rightarrow \infty$ this critical value is majorated by

$$Ro(\beta) = \frac{1 + 4\beta^4 - (1 + 2\beta^2)\sqrt{1 + 4\beta^4}}{2\beta^2}, \quad (45)$$

with the maximum at the well-known Liu limit $Ro_c = 2 - 2\sqrt{2} \simeq -0.828$ when $\beta = \sqrt{2}/2 \simeq 0.707$ [51, 54]. The line (45) is shown red in Fig. 7(left). Nevertheless, at small but finite Pm , the HMRI domain shown in dark grey in Fig. 7(left) can exceed the Liu limit for some choice of Ha and Re .

To understand how far beyond the Liu limit HMRI can exist, we show in Fig. 8 a typical critical surface $m_4 = 0$ in the (Pm, Re^{-1}, Ro) -space for the special parameter choice $Ha = 15$ and $\beta = 0.7$. On the Ro -axis we find a self-intersection and two Whitney umbrella singularities at its ends. At the upper singular point, i.e. exactly at $Pm = 0$, the critical Rossby number is given by Eq. (44) in the limit $Re \rightarrow \infty$.

In Fig. 8 we see that the case with $Pm = 0$ is connected to the case $Pm \neq 0$ by the Plücker conoid singularity, quite similar as it was discussed for the paradox of Velikhov and Chandrasekhar. Interestingly, Ro_c for the onset of HMRI can indeed increase when Pm departs from zero which happens along curved pockets of HMRI. The two side bumps of the curve $Re^{-1}(Pm)$ in a horizontal slice of the surface correspond to the domains of the *essential HMRI* while the central hill marks the *helically modified SMRI* domain, according to

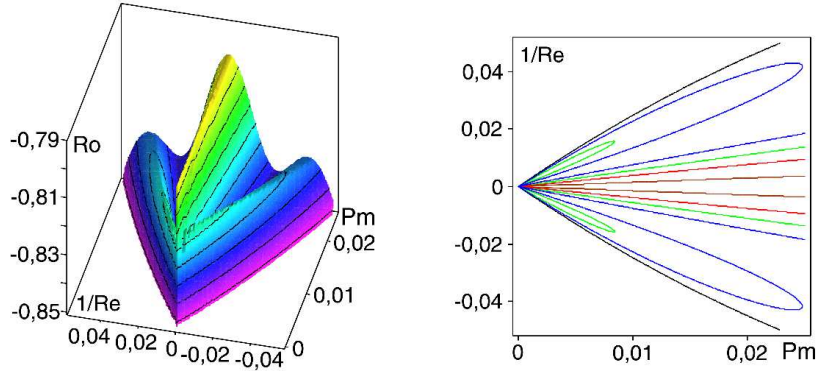


Fig. 9 (left) The critical Rossby number for $Lu = 0.5$ and $\beta = 0.6$ in the (Pm, Re^{-1}, Ro) -space and (right) its cross-sections in the (Pm, Re^{-1}) -plane for (black) $Ro = -0.842$, (blue) $Ro = -0.832$, (green) $Ro = -0.822$, (red) $Ro = -0.812$, (brown) $Ro = -0.802$ [60].

the classification introduced in [54], see also Fig. 7(right). For small Pm the essential HMRI occurs at higher Ro than the helically modified SMRI, while for some finite value of Pm the central hill and the side bumps get the same value of Ro_c . Most remarkably, there is a value of Ro_c at which the two side bumps of the curve $Re^{-1}(Pm)$ disappear completely. This is the maximal possible value for the essential HMRI, at least at the given β and Ha . Now we can ask: how does this limit behave if we send Ha to infinity, and to which value of Lu does this correspond?

Actually, with the increase in Ha the stability boundary preserves its shape and simultaneously it compresses in the direction of zero Pm . Substituting $Ha = LuPm^{-1/2}$ into the equations (42), we plot again the surface $m_4 = 0$ in the (Pm, Re^{-1}, Ro) -space, but now for a given β and Lu , Fig. 9(left).

The corresponding cross-sections of the instability domain in the (Re^{-1}, Pm) -plane are shown in Fig. 9(right). At a given value of Ro there exist three domains of instability with the boundaries shown in blue and green. Two sub-domains that have a form of a petal correspond to the HMRI. They are bounded by closed curves with a self-intersection singularity at the origin. They are also elongated in a preferred direction that in the (Re^{-1}, Pm) -plane corresponds to a limited range of the magnetic Reynolds number $Rm = PmRe$. The central domain, which corresponds to the helically modified SMRI, has a similar singularity at the origin and is unbounded in the positive Pm -direction. In comparison with the central domain where $Rm > 1$, within the side petals $Rm < 1$.

Now we reconsider again the limit $Pm \rightarrow 0$, while keeping Lu as a free parameter. At the origin all the boundaries of the petals can be approximated by the straight lines $Pm = RmRe^{-1}$. Substituting this expression into equation $m_4 = 0$, we find that the only term that does not depend on Pm is a polynomial

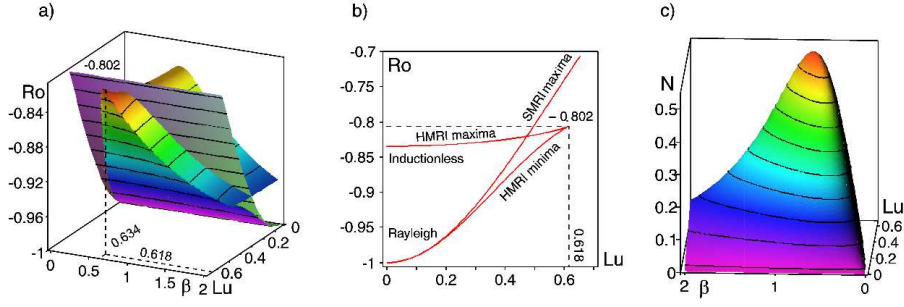


Fig. 10 (a) Discriminant surface in the (Lu, β, Ro) -space and (b) its cross-section [60] at $\beta = 0.634$. (c) Interaction parameter $N = Lu^2 Rm^{-1}$ at the essential HMRI maxima.

$Q(Rm, Lu, \beta, Ro) = p_0 + p_1 Rm^2 + p_2 Rm^4 + p_3 Rm^6$, with the coefficients

$$\begin{aligned}
 p_0 &= Lu^4(4\beta^4 Lu^2 + 2\beta^2 + 4Lu^2\beta^2 + 1)^2 \\
 p_1 &= 4(-\beta^2(1 + 20Lu^4\beta^2 + 2Lu^4 + 8\beta^2 Lu^6 \\
 &\quad + 16\beta^6 Lu^6 + 24Lu^6\beta^4 + 4Lu^2 + 8\beta^2 Lu^2 + 20\beta^4 Lu^4)Ro^2 \\
 &\quad + (16Lu^6\beta^4 + 16\beta^6 Lu^2 + Lu^2 + 4\beta^4 + 16\beta^8 Lu^4 + 1 - 16\beta^8 Lu^6 + 4Lu^2\beta^4)Ro \\
 &\quad + 1 - 8Lu^2\beta^2(Lu^4\beta^2 - \beta^2 + Lu^4 - \beta^2 Lu^2 + Lu^2) \\
 &\quad + 16\beta^6 Lu^2(1 + \beta^2 Lu^2 + Lu^2 + Lu^4) + 4\beta^4 + 2Lu^4) \\
 p_2 &= 16(Lu^4\beta^4 Ro^4 - \beta^2(-2 + 4\beta^4 Lu^4 - 3Lu^2 + 4Lu^4\beta^2)Ro^3 \\
 &\quad + 2\beta^2(3 + 4\beta^2 + 6\beta^4 Lu^4 + 4Lu^2 + 16\beta^2 Lu^2 + 3Lu^4 + 8Lu^2\beta^4 + 12Lu^4\beta^2)Ro^2 \\
 &\quad + (32\beta^4 Lu^4 + 16\beta^4 + 40Lu^2\beta^4 + 2 + 2Lu^2 + 4\beta^2 + 32\beta^6 Lu^4 + 32\beta^6 Lu^2)Ro \\
 &\quad + 2 + 4Lu^4\beta^2 + 8Lu^2\beta^4 + 16\beta^6 Lu^2 + 8\beta^4 + 16\beta^6 Lu^4 + Lu^4 + 4\beta^4 Lu^4) \\
 p_3 &= 64((2Ro\beta^2 + 1)^2 + 8Ro\beta^4 + 4\beta^4 + 3Ro^2\beta^2 - Ro^3\beta^2)(Ro + RoLu^2 + 1). \quad (46)
 \end{aligned}$$

The roots of the polynomial are coefficients Rm of the linear approximation to the instability domains at the origin in the (Re^{-1}, Pm) -plane. Simple roots mean non-degenerate self-intersection of the stability boundary at the origin. Double roots correspond to a degeneration of the angle of the self-intersection when it collapses to zero which happens only at the maximal critical Rossby number, Fig. 9(left). In the (Lu, β, Ro) -space a set of points that correspond to multiple roots of the polynomial Q is given by the discriminant surface $64\Delta^2 p_0 p_3 = 0$, where

$$\Delta(Lu, \beta, Ro) := 18p_0 p_1 p_2 p_3 - 4p_1^3 p_3 + p_1^2 p_2^2 - 4p_0 p_2^3 - 27p_0^2 p_3^2. \quad (47)$$

The surface $p_3 = 0$ consists of a sheet $Ro = -(1 + Lu^2)^{-1}$ corresponding to the doubly degenerate infinite values of Rm at the maxima of the helically modified SMRI. It smoothly touches along the β -axis the surface $\Delta = 0$ that consists of two smooth sheets that touch each other along a spatial curve — the cuspidal edge — corresponding to triple roots of the polynomial Q , Fig. 10(a).

Every point on the upper sheet of the surface $\Delta = 0$ represents a degenerate linear approximation to the essential HMRI domain and therefore a maximal Ro at the corresponding values of β and Lu . Numerical optimization results in the new ultimate limit for HMRI $Ro_c \simeq -0.802$ at $Lu \simeq 0.618$, $\beta \simeq 0.634$, and $Rm \simeq 0.770$, see Fig. 10(b). This new limit of Ro_c on the cuspidal edge is smoothly connected to the inductionless Liu limit by the upper sheet of the discriminant surface, which converges to the curve (45) when $Lu = 0$. We point out that the new limit is achieved at $Ha \rightarrow \infty$ when the optimal Pm tends to zero in such a way that $Lu \simeq 0.618$. Figure 10(c) shows the behaviour of the so-called interaction parameter (or Elsasser number) $N = Lu^2/Rm$ for the HMRI sheet. It is remarkable that, at $Lu = 0$, HMRI starts to work already at $N = 0$. This can be explained by the observation that the optimal value for HMRI corresponds to $NHa = Lu^3/(Rm\sqrt{Pm}) = 1/(1 + 2^{-1/2}) = 0.586$, [54]. Later, for increasing Lu , the optimal N acquires final values, passes through its maximum and at $Lu \simeq 0.618$ and $\beta \simeq 0.634$ it terminates at $N = 0.496$.

4 Conclusion

Motivated by the well-established theory of dissipation induced instabilities [61, 62, 63, 64, 65, 66, 67, 68, 69, 70, 71, 72], we have resolved the two paradoxes of SMRI and HMRI in the limits of infinite and zero magnetic Prandtl number, respectively, by establishing their sharp correspondence to singularities on the instability thresholds. In either case, the local Plücker conoid structure has been identified as responsible for the non-uniqueness of the critical Rossby number, and its crucial dependence on the Lundquist number. For HMRI, we have found an extension of the former Liu limit $Ro_c \simeq -0.828$ (valid for $Lu = 0$) to a somewhat higher value $Ro \simeq -0.802$ at $Lu = 0.618$ which is, however, still below the Kepler value. A remarkable feature of HMRI is an abrupt disappearance of its extrema at a finite Lundquist number (see Fig. 9). The discussion of possible physical consequences of this discontinuity, for example as an alternative way of explaining the so-called Quasi-Periodic-oscillations (QPO) [84, 85], must be left for future work.

Acknowledgments

Financial support from the Alexander von Humboldt Foundation and the DFG in frame of STE 991/1-1 and of SFB 609 is gratefully acknowledged.

References

1. Piau, J. M., Bremond, M., Couette, J. M., and Piau, M., Maurice Couette, one of the founders of rheology, *Rheol. Acta*, 33, 357–368 (1994).
2. Couette, M., Sur un nouvel appareil pour l'étude du frottement des fluids, *Comptes Rend.*, 107, 388–390 (1888).

3. Couette, M., Etudes sur le frottement des liquides, *Ann. Chim. Phys.*, 6(21), 433–510 (1890).
4. Velikhov, E. P., Stability of an ideally conducting liquid flowing between cylinders rotating in a magnetic field, *Sov. Phys. JETP-USSR*, 9(5), 995–998 (1959).
5. Taylor, G. I., Stability of a viscous liquid contained between two rotating cylinders, *Phil. Trans. R. Soc. Lond. A*, 223, 289–343 (1923).
6. Balbus, S. A. & Hawley, J. F., A powerful local shear instability in weakly magnetized disks: I. Linear analysis, *ApJ*, 376, 214–233 (1991).
7. Mallock, A., Determination of the viscosity of water, *Proc. R. Soc. Lond.*, 45, 126–132 (1888 - 1889).
8. Mallock, A., Experiments on fluid viscosity, *Phil. Trans. R. Soc. Lond. A*, 187, 41–56 (1896).
9. Donnelly, R. J., Taylor-Couette flow: The early days. *Phys. Today*, 44, 32–39 (1991).
10. Rayleigh, J. W. S., On the dynamics of revolving fluids, *Proc. R. Soc. Lond. A*, 93, 148–154 (1917).
11. Chossat, P., Iooss, G., *The Couette-Taylor Problem*, Springer, New-York (1994).
12. Simites, G. J., Hodges, D.H., *Fundamentals of structural stability*, Elsevier (2006).
13. Chandrasekhar, S., The stability of viscous flow between rotating cylinders in the presence of a magnetic field, *Proc. R. Soc. London A*, 216(1126), 293–309 (1953).
14. Alfvén, H., Existence of electromagnetic-hydrodynamic waves, *Nature*, 150(3805), 405–406 (1942).
15. Balbus, S. A., Magnetorotational instability, *Scholarpedia*, 4(7), 2409 (2009).
16. Chandrasekhar, S., The stability of non-dissipative Couette flow in hydromagnetics, *Proc. Natl. Acad. Sci. U.S.A.*, 46, 253–257 (1960).
17. Ji, H., Goodman, J., Kageyama, A., Magnetorotational instability in a rotating liquid metal annulus, *Mon. Not. R. Astron. Soc.* 325, L1–L5 (2001).
18. Rüdiger, G., Zhang, Y., MHD instability in differentially-rotating cylindric flows, *Astronomy and Astrophysics* 378, 302–308 (2001).
19. Willis, A. P., Barenghi, C. F., Magnetic instability in a sheared azimuthal flow, *Astronomy and Astrophysics* 388, 688–691 (2002).
20. Dubrulle, B., et al., Stability and turbulent transport in Taylor-Couette flow from analysis of experimental data, *Phys. Fluids* 17, 095103 (2005).
21. Acheson D. J., Hide, R., Hydromagnetics of rotating fluids, *Rep. Prog. Phys.* 36, 159–221 (1973).
22. Balbus, S. A., Enhanced angular momentum transport in accretion disks, *Ann. Rev. Astron. Astroph.*, (41), 555–597 (2003).
23. Tassoul, J.-L. and Tassoul, M., *A Concise History of Solar and Stellar Physics*, Princeton University Press, Princeton, NJ (2004).
24. Velikhov, E. P., Magnetic geodynamics, *JETP Letters*, 82(11), 690–695 (2005).
25. Shalybkov, D. A., Hydrodynamic and hydromagnetic stability of the Couette flow, *Physics-Uspeski*, 52(9), 915–935 (2009).
26. Goedbloed, H., Keppens, R. and Poedts, S. *Advanced Magnetohydrodynamics*, Cambridge University Press, Cambridge, UK (2010).
27. Balbus, S. A., Hawley J. F., Instability, turbulence, and enhanced transport in accretion disks, *Rev. Mod. Phys.*, 70(1), 1–53 (1998).
28. Beletsky, V. V., Levin, E. M., *Dynamics of Space Tether Systems*, Volume 83 - Advances in the Astronautical Sciences, American Astronautical Society, San Diego, CA (1993).
29. Breakwell, J. V., Stability of an orbiting ring, *J. Guid. and Contr.*, 4(22), 197–200 (1981).
30. Beletsky, V. V., Levin, E. M., Stability of a ring of connected satellites, *Acta Astron.*, 12(10), 765–769 (1985).
31. Hill, G. W., Researches in the Lunar Theory, *Am. J. Math.*, 1(1), 5–26 (1878).
32. Clohessy, W.H., Wiltshire, R.S., Terminal guidance system for satellite rendezvous, *J. of the Aerospace Sciences*, 27(9), 653–658, 674 (1960).
33. Herron, I., Onset of instability in hydromagnetic Couette flow, *Anal. Appl.*, 2, 145 (2004).
34. Sisan, D. R., et al., Experimental observation and characterization of the magnetorotational instability, *Phys. Rev. Lett.* 93, 114502 (2004).
35. Hollerbach, R., Non-axisymmetric instabilities in magnetic spherical Couette flow, *Proc. R. Soc. A* 465, 2003–2013 (2009).

36. Gissinger, C. Ji, H., and Goodman, J., Instabilities in magnetized spherical Couette flow, *Phys. Rev. E* 84, 026308 (2011).
37. Nornberg, M. D., Ji, H., Schartman, E., Roach, A., Goodman, J., Observation of magnetocoriolis waves in a liquid metal Taylor-Couette experiment, *Phys. Rev. Lett.* 104(7), 074501 (2010).
38. Ji, H., Current status and future prospects for laboratory study of angular momentum transport relevant to astrophysical disks, *Advances in Plasma Astrophysics* (A. Bonanno, E. de Gouveia Dal Pino, A. G. Kosovichev, eds.), *Proceedings IAU Symposium No. 274*, 18–25 (2010).
39. Paoletti, M. S. and Lathrop, D. P., Angular Momentum Transport in Turbulent Flow between Independently Rotating Cylinders, *Phys. Rev. Lett.* 106, 024501 (2011).
40. Balbus, S., A turbulent matter, *Nature* 470, 475–476 (2011).
41. Hollerbach, R., & Rüdiger, G., New type of magnetorotational instability in cylindrical Taylor-Couette flow, *Phys. Rev. Lett.* 95, 124501 (2005).
42. Rüdiger, G., Gellert, M., Schultz, M., Hollerbach, R., Dissipative Taylor-Couette flows under the influence of helical magnetic fields, *Physical Review E*, 82(1), 016319 (2010).
43. Stefani, F., Gundrum, Th., Gerbeth, G., Rüdiger, G., Schultz, M., Szklarski, J., Hollerbach, R. Experimental evidence for magnetorotational instability in a Taylor-Couette flow under the influence of a helical magnetic field, *Phys. Rev. Lett.* 97, 184502 (2006).
44. Rüdiger, G., Hollerbach, R., Stefani, F., Gundrum, Th., Gerbeth, G., Rosner, R. The traveling wave MRI in cylindrical Taylor-Couette flow: comparing wavelengths and speeds in theory and experiment *Astrophys. J. Lett.* 649, L145–L147 (2006).
45. Stefani, F., Gerbeth, G., Gundrum, Th., Szklarski, J., Ruediger, G., Hollerbach, R., Results of a modified PROMISE experiment, *Astron. Nachr.*, 329(7), 652–658 (2008).
46. Stefani, F., Gailitis, A., Gerbeth, G., Magnetohydrodynamic experiments on cosmic magnetic fields *ZAMM-Z. Angew. Math. Mech.*, 88(12), 930–954, (2008).
47. Stefani, F., Gerbeth, G., Gundrum, Th., Hollerbach, R., Priede, J., Rüdiger, G., Szklarski, J., Helical magnetorotational instability in a Taylor-Couette flow with strongly reduced Ekman pumping, *Phys. Rev. E* 80, 066303 (2009).
48. Priede, J. Gerbeth, G., Absolute versus convective helical magnetorotational instability in a Taylor-Couette flow, *Phys. Rev. E* 79, 0463010 (2009).
49. Liu, W., Noise-sustained convective instability in a magnetized Taylor-Couette flow, *Astrophys. J.* 692, 998–1003 (2009).
50. Rüdiger, G., Schultz, M., Helical magnetorotational instability of Taylor-Couette flows in the Rayleigh limit and for quasi-Kepler rotation, *Astron. Nachr.*, 329(7), 659–666 (2008).
51. Liu, W., Goodman, J., Herron, I., & Ji, H., Helical magnetorotational instability in magnetized Taylor-Couette flow, *Phys. Rev. E.*, 74, 056302 (2006).
52. Lakhin, V. P. & Velikhov, E. P., Instabilities of highly-resistive rotating liquids in helical magnetic fields, *Phys. Lett. A*, 369, 98–106 (2007).
53. Priede, J., Grants, I. & Gerbeth, G., Inductionless magnetorotational instability in a Taylor-Couette flow with a helical magnetic field, *Phys. Rev. E*, 75, 047303 (2007).
54. Kirillov, O. N., Stefani, F., On the relation of standard and helical magnetorotational instability, *ApJ*, 712(1), 52–68, (2010).
55. Seyranian, A. P., Kirillov, O. N., Mailybaev, A. A. Coupling of eigenvalues of complex matrices at diabolic and exceptional points, *J. Phys. A: Math. Gen.*, 38(8), 1723–1740 (2005).
56. Rüdiger, G., and Hollerbach, R., Comment on 'Helical magnetorotational instability in magnetized Taylor-Couette flow', *Phys. Rev. E* 76, 068301 (2007).
57. Balbus, S.A. and Henri, P., On the magnetic Prandtl number behaviour of accretion disks, *Astrophys. J.* 674, 408–414 (2008).
58. Lesur, G, Longaretti, P.-Y., Impact of dimensionless numbers on the efficiency of magnetorotational instability induced turbulent transport, *Mon. Not. Roy. Astron. Soc.* 378, 1471–1480 (2007).
59. Umurhan, O. M., Low magnetic-Prandtl number flow configurations for cold astrophysical disk models: speculation and analysis, *Astron. Astrophys.* 513, A47 (2010).
60. Kirillov, O.N., Stefani, F., Paradoxes of magnetorotational instability and their geometrical resolution, *Phys. Rev. E.* 84, 036304 (2011).
61. Bottema, O., The Routh-Hurwitz condition for the biquadratic equation, *Indag. Math.* 18, 403–406 (1956).

62. Arnold, V. I., On matrices depending on parameters, *Russ. Math. Surv.* 26, 29–43 (1971).
63. Levantovskii, L. V., The boundary of a set of stable matrices, *Usp. Mat. Nauk* 35(2), 212–214 (1980).
64. Levantovskii, L. V., Singularities of the boundary of a region of stability, (Russian) *Funktsional. Anal. i Prilozhen.* 16(1), 44–48, 96 (1982).
65. Van Gils, S. A., Krupa, M., Langford, W. F., Hopf bifurcation with non-semisimple 1:1 resonance, *Nonlinearity* 3, 825–850 (1990).
66. Bloch, A. M., Krishnaprasad, P. S., Marsden, J. E., and Ratiu, T. S., Dissipation-induced instabilities, *Annales Inst. Henri Poincaré*, 11(1), 37–90 (1994).
67. Hoveijn, I., and Ruijgrok M., The stability of parametrically forced coupled oscillators in sum resonance, *Z. Angew. Math. Phys.*, 46, 384–392 (1995).
68. Langford, W. F., Hopf Meets Hamilton Under Whitney's Umbrella, in *IUTAM Symposium on Nonlinear Stochastic Dynamics. Proceedings of the IUTAM Symposium, Monticello, IL, USA, August 2630, 2002, Solid Mech. Appl.* 110, edited by S.N. Namachchivaya et al., pp. 157–165, Kluwer, Dordrecht, (2003).
69. Kirillov, O. N., Destabilization paradox. *Doklady Physics*, 49(4), 239–245 (2004).
70. Kirillov, O. N., Gyroscopic stabilization in the presence of nonconservative forces. *Doklady Mathematics*, 76, 780–785 (2007).
71. Krechetnikov, R. & Marsden, J. E., Dissipation-induced instabilities in finite dimensions, *Rev. Mod. Phys.* 79, 519–553 (2007).
72. Kirillov, O. N., Verhulst, F., Paradoxes of dissipation-induced destabilization or who opened Whitney's umbrella? *ZAMM-Z. angew. Math. Mech.*, 90(6), 462–488 (2010).
73. Rüdiger, G., Hollerbach, R., Gellert, M. and Schultz, M., The azimuthal magnetorotational instability (AMRI), *Astron. Nachr.* 328(10), 1158–1161 (2007).
74. Rüdiger, G., Schultz, M., and Gellert, M., The Tayler instability of toroidal magnetic fields in a columnar gallium experiment, *Astron. Nachr.* 332(1), 17 – 23 (2011).
75. Kirillov, O. N., Guenther, U., Stefani, F., Determining role of Krein signature for three dimensional Arnold tongues of oscillatory dynamos. *Phys. Rev. E*, 79(1), 016205 (2009).
76. Drazin, P. G., Reid, W. H., *Hydrodynamic stability*, Cambridge Univ. Press, Cambridge, UK (1981).
77. Marden, M., *Geometry of Polynomials*, AMS, Providence, RI, (1966).
78. Eckhardt, B., Yao, D. Local stability analysis along Lagrangian paths, *Chaos, Solitons & Fractals*, 5(11), 2073–2088 (1995).
79. Berger, M., Gostiaux, B., *Differential Geometry: Manifolds, Curves and Surfaces*, Grad. Texts in Math., vol. 115, Springer, Berlin (1988).
80. Hoveijn, I., Kirillov O. N., Singularities on the boundary of the stability domain near 1:1-resonance, *J. Diff. Eqns.*, 248(10), 2585–2607 (2010).
81. Synge, J. L., The stability of heterogeneous liquids, *Trans. R. Soc. Can.* 27, 1–18 (1933).
82. Gebhardt, T., Grossmann, S., The Taylor-Couette eigenvalue problem with independently rotating cylinders, *Z. Phys. B* 90, 475490 (1993).
83. Bilharz, H., Bemerkung zu einem Satze von Hurwitz, *Z. Angew. Math. Mech.* 24, 77–82 (1944).
84. Remillard, R. A., McClintock J. E., X-ray properties of black-hole binaries, *Ann. Rev. Astron. Astrophys.* 44, 49–92 (2006).
85. Lesaffre, P., Balbus, S. A., Latter, H., A comparison of local simulations and reduced models of MRI-induced turbulence, *Mon. Not. Roy. Astron.* 394, 715–729 (2009).